Commun. Comput. Phys.
doi: 10.4208/cicp.230113.140814a

Vol. **17**, No. 2, pp. 458-486
February 2015

Mixed Spectral Element Method for 2D Maxwell's Eigenvalue Problem

Na Liu[1], Luis Tobón[2,3], Yifa Tang[4] and Qing Huo Liu[2,*]

[1] *Institute of Electromagnetics and Acoustics, Xiamen University, Xiamen, 361005, P.R. China.*
[2] *Department of Electrical and Computer Engineering, Duke University, Durham, NC, 27708, USA.*
[3] *Departamento de Ciencias e Ingeniería de la Computación, Pontificia Universidad Javeriana, Cali, Colombia.*
[4] *LSEC, ICMSEC, Academy of Mathematics and Systems Science, Chinese Academy of Sciences, Beijing 100190, P.R. China.*

Received 23 January 2013; Accepted (in revised version) 14 August 2014

Communicated by Wei Cai

Abstract. It is well known that conventional edge elements in solving vector Maxwell's eigenvalue equations by the finite element method will lead to the presence of spurious zero eigenvalues. This problem has been addressed for the first order edge element by Kikuchi by the mixed element method. Inspired by this approach, this paper describes a higher order mixed spectral element method (mixed SEM) for the computation of two-dimensional vector eigenvalue problem of Maxwell's equations. It utilizes Gauss-Lobatto-Legendre (GLL) polynomials as the basis functions in the finite-element framework with a weak divergence condition. It is shown that this method can suppress all spurious zero and nonzero modes and has spectral accuracy. A rigorous analysis of the convergence of the mixed SEM is presented, based on the higher order edge element interpolation error estimates, which fully confirms the robustness of our method. Numerical results are given for homogeneous, inhomogeneous, L-shape, coaxial and dual-inner-conductor cavities to verify the merits of the proposed method.

AMS subject classifications: 78M10, 78M22

Key words: Maxwell eigenvalues, spectral element method, spurious eigenvalues.

*Corresponding author. *Email addresses:* liuna@xmu.edu.cn (N. Liu), let12@duke.edu (L. Tobón), tyf@lsec.cc.ac.cn (Y. Tang), qhliu@duke.edu (Q. H. Liu)

 ©2015 Global-Science Press

https://doi.org/10.4208/cicp.230113.140814a Published online by Cambridge University Press

1 Introduction

The computation of eigenvalues in Maxwell's equations is of fundamental importance in computational electromagnetics. Since nodal based finite element method was introduced to electrical engineering by Silvester in 1969 [1], it has been shown that the nodal based finite element method has several advantages in solving homogeneous waveguide problems, but in solving inhomogeneous waveguide problems it yields spurious modes with nonzero eigenvalues. Much effort has been made to reduce or eliminate this unwanted numerical behavior due to the presence of spurious modes [2]. Rahman and Winkler observed that spurious modes do not satisfy the zero divergence condition on the electric or magnetic field and suggested a penalty function to enforce this condition [3–5]. Unfortunately, this method cannot eliminate the spurious modes completely and leaves the user the task of selecting a suitable penalty function parameter.

The other approach to eliminating spurious modes in the finite element waveguide problem is to find proper finite element approximation functions [2, 6–9]. It is now well-known that employing $\mathbf{H}(\text{curl};\Omega)$-conforming basis functions (also known as edge elements) for the electric field [7,8] can ensure the continuity of tangential field components across an interface between different media, while leaving the normal field components free to jump across such interfaces. With the edge element method there are no spurious modes with nonzero eigenvalues, but the number of spurious modes with zero eigenvalue is equal to the number of nodal points inside the computational domain due to the violation of Gauss's law [10]. Therefore, in order to remove these zero eigenvalues, in addition to using the proper finite element space, the divergence free property (Gauss's law) of the eigenfunction must be enforced. One such successful approach for computing eigenvalues in waveguide problems is to employ $\mathbf{H}(\mathbf{curl};\Omega)$-conforming basis functions to approximate the electric field while imposing the divergence-free condition through the use of a Lagrange multiplier, as suggested by Kikuchi [14].

In the meantime, higher-order methods such as the spectral element method (SEM) [18,19] have also been proposed to solve electromagnetic eigenvalue problems. But these methods also suffer from the presence of spurious zero eigenvalues, even though these methods have a high convergence rate. In this paper, we present the mixed spectral element method (mixed SEM) by applying the divergence free equation in Kikuchi's scheme into the SEM, for which the preliminary results have been shown in [20]. In the SEM, the basis functions are constructed by Gauss-Lobatto-Legendre (GLL) polynomials [18, 19]. The accuracy increases exponentially with increasing the order of GLL basis functions, while the number of degrees of freedom increases slowly. The convergence of this higher-order mixed SEM is proved under the stronger regularity assumptions based on the interpolation estimates for GLL edge elements and the abstract spectral theory in mixed form [10,11,13,23]. We apply this mixed spectral element method to the two-dimensional vector Maxwell TEz eigenvalue problem and carry out numerical experiments on a homogeneous cavity, an inhomogeneous cavity, a L-shape singular cavity, a coaxial cavity and a two PEC cavity to validate this method. The results show that the mixed spec-

https://doi.org/10.4208/cicp.230113.140814a Published online by Cambridge University Press

tral element method is free of zero and nonzero spurious eigenmodes and has spectral accuracy with analytic eigenvalues.

The rest of the paper is organized as follows. In Section 2, we introduce the variational formulation and the abstract assumptions of the mixed SEM under which the exponential convergence of the eigensolutions can be proved. The brief description of the basis functions and the *hp*-version interpolation estimates of mixed SEM is given in Section 3. Moreover, the properties of the mixed SEM finite element spaces yield the convergence. A series of numerical experiments confirming the good behavior of the mixed SEM are reported in Section 4.

2 Mixed SEM formulation

We consider the domain $\Omega\in\mathbb{R}^2$ and the 2D vector TEz Maxwell's eigenvalue problem: find the eigenvalues $k^2\in\mathbb{R}$ and the electrical field $\mathbf{u}\neq 0$ satisfying

$$\nabla\times\mu_r^{-1}\nabla\times\mathbf{u}=k^2\epsilon_r\mathbf{u}, \quad \text{in } \Omega, \tag{2.1a}$$

$$\nabla\cdot\epsilon_r\mathbf{u}=0, \quad \text{in } \Omega, \tag{2.1b}$$

$$\mathbf{u}\times\mathbf{n}=0, \quad \text{on } \partial\Omega, \tag{2.1c}$$

where we assume a perfectly conducting boundary condition, and ϵ_r and μ_r denote the relative dielectric permittivity and magnetic permeability tensors, respectively. $\mathbf{n}$ is the outward unit normal.

Without the divergence term (2.1b), the variational formulation of the problem (2.1) is: find $\lambda=k^2\in\mathbb{R}$ and $\mathbf{u}\in\mathbf{H}_0(\text{curl};\Omega)$ with $\mathbf{u}\neq 0$ such that

$$(\mu_r^{-1}\nabla\times\mathbf{u},\nabla\times\mathbf{v})=\lambda(\epsilon_r\mathbf{u},\mathbf{v}) \qquad \forall\,\mathbf{v}\in\mathbf{H}_0(\text{curl};\Omega), \tag{2.2}$$

where

$$\mathbf{H}_0(\text{curl};\Omega)=\left\{\mathbf{v}\in\mathbf{L}^2(\Omega):\ \nabla\times\mathbf{v}=\frac{\partial v_2}{\partial x_1}-\frac{\partial v_1}{\partial x_2}\in L^2(\Omega),\ \ \mathbf{v}\times\mathbf{n}=0\ \text{ on }\partial\Omega\right\},$$

and $\mathbf{L}^2(\Omega)=(L^2(\Omega))^2$. It is easy to observe that (2.2) has non-physical zero eigenvalues and the corresponding eigenspace $\mathbf{u}=\nabla\varphi$, where $\varphi\in\mathbf{H}_0^1(\Omega)$, has an infinite dimension, and the number of spurious zero eigenvalues is equal to the number of internal nodes in the finite element mesh. Therefore, it is difficult to find the real physical zero eigenvalues from all of numerical approximation to zero eigenvalues when the Maxwell eigenvalue problem does have its zero eigenvalues [15]. In this paper, besides using the curl-conforming finite element space, in order to suppress the spurious zero eigenvalues we consider the divergence condition (2.1b). The natural variational formulation of (2.1) is: find $\lambda\in\mathbb{R}$ and non-trivial $\mathbf{u}\in\mathbf{H}_0(\text{curl};\Omega)$ such that

$$(\mu_r^{-1}\nabla\times\mathbf{u},\nabla\times\mathbf{v})=\lambda(\epsilon_r\mathbf{u},\mathbf{v}) \qquad \forall\,\mathbf{v}\in\mathbf{H}_0(\text{curl};\Omega), \tag{2.3a}$$

$$(\epsilon_r\mathbf{u},\nabla q)=0 \qquad \forall\, q\in\mathbf{H}_0^1(\Omega). \tag{2.3b}$$

https://doi.org/10.4208/cicp.230113.140814a Published online by Cambridge University Press

Here we enforce the divergence term as a Lagrange multiplier which was introduced by Kikuchi [14] for the mixed finite element method. The mixed formulation associated with (2.1) is: find $\lambda\in\mathbb{R}$ and non-trivial $\mathbf{u}\in\mathbf{H}_0(\text{curl};\Omega)$, $p\in\mathbf{H}_0^1(\Omega)$ such that

$$(\mu_r^{-1}\nabla\times\mathbf{u},\nabla\times\mathbf{v})+(\nabla p,\epsilon_r\mathbf{v})=\lambda(\epsilon_r\mathbf{u},\mathbf{v}) \qquad \forall\mathbf{v}\in\mathbf{H}_0(\text{curl};\Omega), \tag{2.4a}$$

$$(\epsilon_r\mathbf{u},\nabla q)=0 \qquad \forall q\in\mathbf{H}_0^1(\Omega), \tag{2.4b}$$

where

$$\mathbf{H}_0^1(\Omega)=\{q\in L^2(\Omega):\ \nabla q\in\mathbf{L}^2(\Omega),\ q=0 \text{ on } \partial\Omega\}.$$

We can easily find that mixed formulation (2.4) is equivalent to (2.3). By taking $\mathbf{v}=\nabla p$ in (2.4a) and using (2.4b) can get $\nabla p=0$, which shows that all solutions of (2.4) solve Eq. (2.3) as well. Vice versa, it is clear that solutions to (2.3) solve (2.4) with $p=0$. The mixed formulation (2.4) is denoted as the mixed spectral element method (mixed SEM) because we apply the spectral element method to obtain the discrete space $V_h\subset\mathbf{H}_0(\text{curl};\Omega)$ and $Q_h\subset\mathbf{H}_0^1(\Omega)$. Basis functions for the mixed SEM are discussed in the following section.

For all $\mathbf{u},\mathbf{v}\in\mathbf{H}_0(\text{curl};\Omega)$ and $q\in\mathbf{H}_0^1(\Omega)$, here we define the sesquilinear forms

$$a(\mathbf{u},\mathbf{v})=\int_\Omega \mu_r^{-1}\nabla\times\mathbf{u}\cdot\overline{\nabla\times\mathbf{v}}d\mathbf{x},$$

$$b(q,\mathbf{u})=\int_\Omega \epsilon_r\mathbf{u}\cdot\overline{\nabla q}d\mathbf{x},$$

$$(\mathbf{u},\mathbf{v})=\int_\Omega \epsilon_r\mathbf{u}\cdot\bar{\mathbf{v}}d\mathbf{x}.$$

Problem (2.4) can be rewritten in the following mixed form: find $\lambda\in\mathbb{R}$, $(\mathbf{u},p)\in\mathbf{H}_0(\text{curl};\Omega)\times\mathbf{H}_0^1(\Omega)$ with $(\mathbf{u},p)\neq(0,0)$, such that

$$\begin{cases} a(\mathbf{u},\mathbf{v})+b(q,\mathbf{v})=\lambda(\mathbf{u},\mathbf{v}) & \forall\mathbf{v}\in\mathbf{H}_0(\text{curl};\Omega),\\ \overline{b(q,\mathbf{u})}=0 & \forall q\in\mathbf{H}_0^1(\Omega).\end{cases} \tag{2.5}$$

Now we introduce the kernel of $\nabla\cdot$, that is

$$\mathbb{K}=\{\mathbf{v}\in\mathbf{H}_0(\text{curl};\Omega):\ b(q,\mathbf{v})=0,\ \forall q\in\mathbf{H}_0^1(\Omega)\}. \tag{2.6}$$

Let $T\in\mathfrak{L}(\mathbf{L}^2(\Omega),\mathbf{L}^2(\Omega))$ be the resolvent operator associated with (2.5) and defined as follows. For all $\mathbf{f}\in\mathbf{L}^2(\Omega)$, $T\mathbf{f}=\mathbf{u}\in\mathbf{L}^2(\Omega)$, where $\mathbf{u}$ is the first component of the solution of the following problem: find $(\mathbf{u},p)\in\mathbf{H}_0(\text{curl};\Omega)\times\mathbf{H}_0^1(\Omega)$, such that

$$\begin{cases} a(\mathbf{u},\mathbf{v})+b(p,\mathbf{v})=(\mathbf{f},\mathbf{v}) & \forall\mathbf{v}\in\mathbf{H}_0(\text{curl};\Omega),\\ \overline{b(q,\mathbf{u})}=0 & \forall q\in\mathbf{H}_0^1(\Omega).\end{cases} \tag{2.7}$$

We can see that T is compact and self-adjoint (see [10]), then T admits an increasing sequence of real, positive eigenvalues

$$0<\lambda_1<\lambda_2<\cdots<\lambda_n<\cdots, \tag{2.8}$$

https://doi.org/10.4208/cicp.230113.140814a Published online by Cambridge University Press

each eigenvalue related to a finite dimensional eigenspace.

Let us state the regularity result we need in order to carry out our analysis in the following section.

Assumption 2.1 (Regularity assumption)**.** For all $\mathbf{f}\in\mathbf{L}^2(\Omega)$ the solution $\mathbf{u}$ of problem (2.7) satisfies

$$\begin{aligned}&\mathbf{u}\in(\mathbf{H}^s(\Omega))^2 \qquad \text{for some} \quad s>1,\\ &\nabla\times\mathbf{u}\in\mathbf{H}^r(\Omega) \qquad \text{for some} \quad r>1/2.\end{aligned}$$

The corresponding discretized formulation for (2.2) is to determine $\lambda\in\mathbb{R}$ and $\mathbf{u}_h\in V_h\subset\mathbf{H}_0(\text{curl};\Omega)$ with $\mathbf{u}_h\neq 0$ such that

$$(\mu_r^{-1}\nabla\times\mathbf{u}_h,\nabla\times\mathbf{v}_h)=\lambda(\epsilon_r\mathbf{u}_h,\mathbf{v}_h) \qquad \forall\,\mathbf{v}_h\in V_h. \tag{2.9}$$

Meanwhile, the discrete form of (2.4) is to get $\lambda\in\mathbb{R}$ and non-trivial $\mathbf{u}_h\in V_h\subset\mathbf{H}_0(\text{curl};\Omega)$, $p_h\in Q_h\subset\mathbf{H}_0^1(\Omega)$ satisfying

$$\begin{cases}(\mu_r^{-1}\nabla\times\mathbf{u}_h,\nabla\times\mathbf{v}_h)+(\nabla p_h,\epsilon_r\mathbf{v}_h)=\lambda(\epsilon_r\mathbf{u}_h,\mathbf{v}_h) & \forall\,\mathbf{v}_h\in V_h,\\ (\epsilon_r\mathbf{u}_h,\nabla q_h)=0 & \forall\,q_h\in Q_h.\end{cases} \tag{2.10}$$

In order to analyze the convergence of the discrete mixed finite element form to the continuous form we apply the corresponding abstract theory developed in [11]. Firstly we consider the discretization of the resolvent operator $T_h:\ \mathbf{L}^2(\Omega)\to V_h$: for all $\mathbf{L}^2(\Omega)$, $T_h\mathbf{f}=\mathbf{u}_h\in V_h$, where $\mathbf{u}_h$ is the first component of the solution of the problem: find $(\mathbf{u}_h,p_h)\in V_h\times Q_h$, such that

$$\begin{cases}a(\mathbf{u}_h,\mathbf{v}_h)+b(p_h,\mathbf{v}_h)=(\mathbf{f},\mathbf{v}_h) & \forall\,\mathbf{v}_h\in V_h,\\ \overline{b(q_h,\mathbf{u}_h)}=0 & \forall\,q_h\in Q_h.\end{cases} \tag{2.11}$$

The compact and self-adjoint operator like T, a sufficient and necessary condition is shown in [12] to have the convergence of the spectrum is the uniform convergence in the operator norm, that is:

$$\lim_{h\to 0}\|T-T_h\|_{\mathfrak{L}(\mathbf{L}^2(\Omega),\mathbf{L}^2(\Omega))}=0. \tag{2.12}$$

The following assumptions on the finite element space are useful in the analysis of the convergence, see [11] for the details.

Assumption 2.2 (Ellipticity on the discrete kernel)**.** There exists $\alpha>0$, independent of h and N, such that

$$a(\mathbf{u}_h,\mathbf{u}_h)\geq\alpha\|\mathbf{u}_h\|_{\text{curl}}^2 \qquad \forall\,\mathbf{u}_h\in\mathbb{K}_h, \tag{2.13}$$

where the discrete kernel $\mathbb{K}_h$ is defined as

$$\mathbb{K}_h=\{\mathbf{u}_h\in V_h \text{ such that } b(q_h,\mathbf{u}_h)=0,\ \forall\,q_h\in Q_h\}. \tag{2.14}$$

https://doi.org/10.4208/cicp.230113.140814a Published online by Cambridge University Press

Assumption 2.3 (Weak approximability)**.** There exists $\rho_1(N,h)$, tending to zero as $N\to\infty$ and $h\to 0$, such that for any $p\in\mathbf{H}_0^1(\Omega)$ it holds

$$\sup_{\mathbf{v}_h\in\mathbb{K}_h}\frac{b(p,\mathbf{v}_h)}{\|\mathbf{v}_h\|_{\text{curl}}}\leq\rho_1(N,h)\|p\|_1. \tag{2.15}$$

Assumption 2.4 (Strong approximability)**.** There exists $\rho_2(N,h)$, tending to zero as $N\to\infty$ and $h\to 0$, such that, for all $\mathbf{u}\in\mathbf{H}_0(\text{curl};\Omega)$ with $\mathbf{u}\in\mathbb{K}$ and satisfying the Regularity Assumption 2.1, there exists $\mathbf{u}^I\in\mathbb{K}_h$ satisfying

$$\|\mathbf{u}-\mathbf{u}^I\|_{\text{curl}}\leq\rho_2(N,h)(\|\mathbf{u}\|_{\mathbf{H}^s}+\|\nabla\times\mathbf{u}\|_{\mathbf{H}^r}). \tag{2.16}$$

Then the following theorem has been proved in [12]:

Theorem 2.1. *Let us assume that Assumptions* 2.2, 2.3 *and* 2.4 *are valid. Then the sequence T_h converges uniformly to T in $\mathfrak{L}(\mathbf{L}^2(\Omega),\mathbf{H}_0(\text{curl};\Omega))$, that is, there exists $\rho_3(N,h)$, tending to zero as $N\to\infty$ and $h\to 0$, such that*

$$\|T\mathbf{f}-T_h\mathbf{f}\|_{\text{curl}}\leq\rho_3(N,h)\|\mathbf{f}\|_0\qquad\forall\,\mathbf{f}\in\mathbf{L}^2(\Omega). \tag{2.17}$$

3 Basis functions and convergence for the mixed SEM

3.1 Basis functions

In order to guarantee the tangential continuity and suppress the non-zero spurious modes, the nullspace of the curl operator must be correctly approximated [6]. Therefore, we apply the mixed-order GLL polynomials as curl-conforming vector basis functions to discretize the electric field $\mathbf{u}_h$ [18]. The definition of the Nth-order vector spectral element space V_h is:

$$V_h=\{\mathbf{v}\in\mathbf{H}_0(\text{curl};\Omega)\mid\mathbf{v}_h|_K\in Q_{N-1,N}\times Q_{N,N-1},\ \forall K\in\Gamma_h\}.$$

We denote K and Γ_h as a quadrilateral element and quadrilateral mesh on Ω. In the reference element $[-1,1]\times[-1,1]$, the mixed-order GLL polynomials vector basis function as shown in Fig. 1 can be written as

$$\begin{cases}\hat{\mathbf{\Phi}}_{ij}^{\xi}=\hat{\xi}\phi_i^{N-1}(\xi)\phi_j^N(\eta),\\ \hat{\mathbf{\Phi}}_{ij}^{\eta}=\hat{\eta}\phi_i^N(\xi)\phi_j^{N-1}(\eta),\end{cases} \tag{3.1}$$

where

$$\phi_m^{(M)}(\xi)=\frac{-(1-\xi^2)L_M'(\xi)}{M(M+1)L_M(\xi_m)(\xi-\xi_m)},\qquad m=0,\cdots,M.$$

https://doi.org/10.4208/cicp.230113.140814a Published online by Cambridge University Press

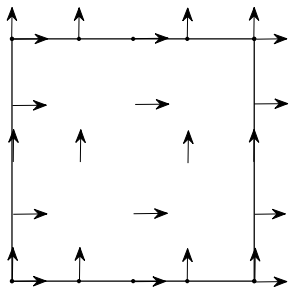


Figure 1: Mixed-order vector curl-conforming basis functions in the reference element with order $N=3$.

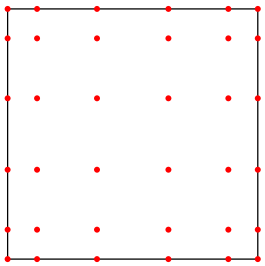


Figure 2: GLL points distribution on the reference element with $N=5$.

$L_M(\xi)$ is the Mth-order Legendre polynomial and $L'_M(\xi)$ is its derivative. $\xi_m \in [-1,1]$ are the zero points of the equation $(1-\xi^2)L'_N(\xi)=0$, which are called GLL points. While the discrete space for $\mathbf{H}_0^1(\Omega)$ is defined as:

$$Q_h = \{q_h \in \mathbf{H}_0^1(\Omega) \mid q_h|_K \in Q_{N,N}(K),\ \forall K \in \Gamma_h\}.$$

The scalar basis functions based on nodal points as shown in Fig. 2 are given by

$$\hat{\Psi}_{ij} = \phi_i^N(\xi)\phi_j^N(\eta).$$

The mixed-order vector basis functions in Fig. 1 are plotted by the associated nodal points. Moreover, we note that the distribution of nodal points in Fig. 2 is denser near the edge of an element than in the middle of the element. Since the field usually changes more drastically at the interface of different materials, this distribution of nodal points has great advantage in simulating systems with discontinuous dielectric materials and can obtain higher accuracy by removing the Runge's phenomenon.

The explicit formulae for the construction of our high order basis functions (3.1) are derived from the curl-conforming polynomial spaces originally proposed by Nédélec [7]. Let $\hat{V}_{\hat{K}}$ denote the curl-conforming basis functions on the reference element, and the $\hat{v} \in \hat{V}_{\hat{K}}$, refer to [7] $\hat{V}_{\hat{K}}$ can decompose into two mutually disjoint subsets such that

$$\hat{V}_{\hat{K}} = \hat{V}_e \cup \hat{V}_f,$$

where the subscripts e and f denote the edges and faces of the reference element, respectively. The vector basis functions in the $\hat{V}_e$ have non-vanishing tangential components along one and only one edge. Meanwhile, the face basis functions in the $\hat{V}_f$ will have non-vanishing tangential components along the face with non tangential components along any edges. The curl-conforming basis functions of polynomial degree equal to N can be written as:

$$\hat{V}_e = \begin{cases} \phi_i^{N-1}(\xi)\phi_j^N(\eta)\hat{\xi}, \\ \phi_j^N(\xi)\phi_i^{N-1}(\eta)\hat{\eta}, \end{cases} \tag{3.2}$$

https://doi.org/10.4208/cicp.230113.140814a Published online by Cambridge University Press

where $j=0,N$ and $i=0,\cdots,N-1$. The subscripts i and j loop over 4 edges of the reference elements. We know $\hat{V}_e$ is tangential to the 1-form edge basis function and the dimension of $\hat{V}_e$ associated with edges of the reference element is equal to $4N$. The curl-conforming face basis functions of polynomial degree N are given by:

$$\hat{V}_f=\begin{cases}\phi_i^{N-1}(\xi)\phi_j^N(\eta)\hat{\xi},\\ \phi_j^N(\xi)\phi_i^{N-1}(\eta)\hat{\eta},\end{cases} \tag{3.3}$$

where $j=1,\cdots,N-1$ and $i=1,\cdots,N$. The indices i and j loop over the face of this 2D reference element and the dimension of the face associating space $\hat{V}_f$ is $2N(N-1)$. Thus, the degrees of freedom for this element can be given in terms of integrals over the edges and faces of $\hat{K}$:

$$\begin{aligned}M_e(\mathbf{u})&=\left\{\int_e \mathbf{u}\cdot\mathbf{t}_e q\,\mathrm{d}s,\ q\in Q_{N-1}(e),\ \text{for each edges of } \hat{K} \text{ and } \mathbf{t}_e \text{ is a unit vector along } e\right\},\\ M_f(\mathbf{u})&=\left\{\int_f \mathbf{u}\cdot\mathbf{q}\,\mathrm{d}A,\ \mathbf{q}\in Q_{N-1,N-2}\times Q_{N-2,N-1}(f)\right\}.\end{aligned} \tag{3.4}$$

The degrees $M(u)=M_e\cup M_f$ are curl-conforming and unisolvent [16]. To keep the tangential component continuous for the vector basis functions $\hat{\mathbf{\Phi}}$ and the continuity of the scalar basis functions $\hat{\Psi}$ under the transformation between reference element and physical element, the covariant mapping is given as [16]

$$\mathbf{\Phi}=(\mathbf{J})^{-1}\hat{\mathbf{\Phi}}, \tag{3.5a}$$

$$\nabla\times\mathbf{\Phi}=\frac{1}{|\mathbf{J}|}\hat{\nabla}\times\hat{\mathbf{\Phi}}, \tag{3.5b}$$

$$\Psi=\hat{\Psi}, \tag{3.5c}$$

$$\nabla\Psi=(\mathbf{J})^{-1}\hat{\nabla}\hat{\Psi}, \tag{3.5d}$$

where $\hat{\mathbf{\Phi}}$ and $\hat{\Psi}$ denote the vector basis function and scalar basis function in the reference element and $\mathbf{J}$ denotes the Jacobian matrix as

$$\mathbf{J}=\begin{bmatrix}\frac{\partial x}{\partial\xi} & \frac{\partial y}{\partial\xi}\\ \frac{\partial x}{\partial\eta} & \frac{\partial y}{\partial\eta}\end{bmatrix}.$$

Defining compound indices for the basis functions of $\mathbf{u}_h$ and p_h in the global system, $m=(\hat{u},i,j)$ and $n=(i,j)$, where $\hat{u}=(\hat{\xi},\hat{\eta})$, the electric field $\mathbf{u}_h$ and p_h in the real space can be expanded as

$$\mathbf{u}_h=\sum_m e_m\mathbf{\Phi}_m,\quad p_h=\sum_n y_n\Psi_n. \tag{3.6}$$

https://doi.org/10.4208/cicp.230113.140814a Published online by Cambridge University Press

3.2 Interpolation error

Before considering the interpolation error of the GLL basis functions, we recall some properties of Legendre polynomials on $[-1,1]$. Let $\{L_j(\xi)\}$, $j=0,1,\cdots$, denote the Legendre polynomials which are orthogonal in the sense that

$$\int_{-1}^{1} L_i(\xi)L_j(\xi) = \frac{2}{2i+1}\delta_{ij}.$$

Any $u \in L^2(\hat{K})$ can be expressed as

$$u(\xi,\eta) = \sum_{i=0}^{\infty}\sum_{j=0}^{\infty} a_{i,j}L_i(\xi)L_j(\eta),$$

using the orthogonality of $\{L_j(\xi)\}$ and their recurrence relation of the derivatives, the zero and r-norm can be written as

$$\|u\|^2_{0,\hat{K}} = \sum_{i=0}^{\infty}\sum_{j=0}^{\infty} \frac{4a^2_{i,j}}{(2i+1)(2j+1)}, \tag{3.7}$$

$$\|u\|^2_{r,\hat{K}} \geq C\sum_{i=0}^{\infty}\sum_{j=0}^{\infty} \frac{a^2_{i,j}(1+i^2+j^2)^r}{(2i+1)(2j+1)}. \tag{3.8}$$

It is well known that for any polynomial $w(x)$ with degree equal to n can be written uniquely in the form $w(x) = \sum_{i=0}^{n} w_i L_i(x)$. Therefore, in order to use the orthogonality of Legendre polynomials and simplify the proof of the interpolation error for GLL polynomials, the interpolation of the first component of $\mathbf{u}$ by GLL polynomials can be also define as

$$\begin{aligned}\hat{\Pi}\hat{u}_1 &= \sum_{i=0}^{N-1}\sum_{j=0}^{N} u_{ij}\phi_i(\xi)\phi_j(\eta) \\ &= \sum_{i=0}^{N-1}\sum_{j=0}^{N} \tilde{u}_{ij}L_i(\xi)L_j(\eta).\end{aligned} \tag{3.9}$$

Thus, the whole interpolation error for GLL basis functions $\|\mathbf{u}-\Pi\mathbf{u}\|$ can be equivalently estimated by the orthogonal Legendre polynomials.

For the curl-conforming basis functions Monk [21] has proved p interpolation error estimates for 3D hexahedral elements using the Nédélec interpolation [7,8]. Refer to [21] here we still give the 2D hp-version interpolation error estimates in the consideration of differences in the convergence rate. In the same way, First we prove the hp-version estimate on the reference element $\hat{K}$. The outline of this proof is to obtain Legendre polynomial expansions of $\hat{\mathbf{u}}$ and $\hat{\Pi}\hat{\mathbf{u}}$ through the definition (3.4). Then we bound the error in terms of standard Sobolev norms.

https://doi.org/10.4208/cicp.230113.140814a Published online by Cambridge University Press

Theorem 3.1. *Let* $\hat{\mathbf{u}}\in(H^s(\hat{K}))^2$, $s>1$ *and let the interpolant* $\hat{\Pi}\hat{\mathbf{u}}$ *be defined by* (3.4)*; then there is a constant* C *independent of* $\hat{\mathbf{u}}$ *and* N *such that*

$$\|\hat{\mathbf{u}}-\hat{\Pi}\hat{\mathbf{u}}\|_{0,\hat{K}}\leq CN^{-(s-\frac{1}{2})}\|\hat{\mathbf{u}}\|_{s,\hat{K}}. \tag{3.10}$$

Applying this theorem and the following result from [22], we can prove an hp-estimate for the global interpolant Π_N.

Lemma 3.1. *let* $\hat{\mathbf{u}}\in(H^s(\hat{K}))^2$ *and* $\mathbf{u}\in(H^s(K))^2$ *for some* $s\geq 0$*. Suppose* $\mathbf{u}$ *and* $\hat{\mathbf{u}}$ *are related by* (3.5a)*; then*

$$\inf_{\hat{\mathbf{w}}\in(Q_{N-1,N-1})^2}\|\hat{\mathbf{u}}-\hat{\mathbf{w}}\|_{s,\hat{K}}\leq Ch_K^{\min(N,s)}\|\mathbf{u}\|_{s,K}. \tag{3.11}$$

We then obtain the following hp-error estimate.

Theorem 3.2. *Let* $\mathbf{u}\in(H^s(\Omega))^2$, $s>1$ *and* $\Pi_N\mathbf{u}:(H^s(\Omega))^2\to V_h$ *be interpolation operator defined by* (3.4)*; then there is a constant* C *independent of* $\hat{\mathbf{u}}$ *and* N *such that*

$$\|\mathbf{u}-\Pi_N\mathbf{u}\|_{0,\Omega}\leq Ch^{\min(N,s)}N^{-(s-\frac{1}{2})}\|\mathbf{u}\|_{s,\Omega}. \tag{3.12}$$

Proof. By Theorem 3.1, for any $K\in\Gamma_h$ we have that for any $\hat{\mathbf{w}}\in(Q_{N-1,N-1})^2$,

$$\|\hat{\mathbf{u}}-\hat{\Pi}\hat{\mathbf{u}}\|_{0,\hat{K}}=\|(\hat{\mathbf{u}}-\hat{\mathbf{w}})-\hat{\Pi}(\hat{\mathbf{u}}-\hat{\mathbf{w}})\|_{0,\hat{K}}\leq CN^{-(s-\frac{1}{2})}\|\hat{\mathbf{u}}-\hat{\mathbf{w}}\|_{s,\hat{K}}.$$

By the scaling argument of (3.5a) and Lemma 3.1, we can get

$$\|\mathbf{u}-\Pi_N\mathbf{u}\|_{0,K}\leq C\|\hat{\mathbf{u}}-\hat{\Pi}\hat{\mathbf{u}}\|_{0,\hat{K}}\leq Ch_K^{\min(N,s)}N^{-(s-\frac{1}{2})}\|\mathbf{u}\|_{s,K}.$$

Then adding this estimate over all element proves the results. □

We now begin to prove Theorem 3.1.

Proof. Let $\hat{\mathbf{u}}=(\hat{u}_1,\hat{u}_2)$; then the interpolant of $\hat{\mathbf{u}}$, denoted by $\hat{\Pi}\hat{\mathbf{u}}$, can be computed component by component:

$$\hat{\Pi}\hat{\mathbf{u}}=(\hat{\Pi}_1\hat{u}_1,\hat{\Pi}_2\hat{u}_2).$$

First we are interested in estimating $\|\hat{u}_1-\hat{\Pi}_1\hat{u}_1\|_{0,\hat{K}}$ instead of $\|\hat{\mathbf{u}}-\hat{\Pi}\hat{\mathbf{u}}\|_{0,\hat{K}}$. Using the degrees of freedom in (3.4), we have the relations for any $\hat{\Pi}_1\hat{u}_1\in Q_{N-1,N}$

$$\int_{-1}^{1}\int_{-1}^{1}(\hat{u}_1-\hat{\Pi}_1\hat{u}_1)(\xi,\eta)\phi(\xi)\zeta(\eta)d\xi d\eta=0 \qquad \forall\phi\in Q_{N-1},\ \zeta\in Q_{N-2}, \tag{3.13}$$

$$\int_{-1}^{1}(\hat{u}_1-\hat{\Pi}_1\hat{u}_1)(\xi,\pm1)\phi(\xi)d\xi=0 \qquad \forall\phi\in Q_{N-1}, \tag{3.14}$$

since $\hat{u}_1\in L^2(\hat{K})$, it has an expansion in terms of Legendre polynomials given by

$$\hat{u}_1=\sum_{i=0}^{\infty}\sum_{j=0}^{\infty}a_{i,j}L_i(\xi)L_j(\eta).$$

https://doi.org/10.4208/cicp.230113.140814a Published online by Cambridge University Press

The interpolant $\hat{\Pi}_1\hat{u}_1$ is expanded as

$$\hat{\Pi}_1\hat{u}_1=\sum_{i=0}^{N-1}\sum_{j=0}^{N}b_{i,j}L_i(\xi)L_j(\eta).$$

Let us consider the coefficients of a_{ij} and b_{ij} by the orthogonality of Legendre polynomials. Taking $\phi(\xi)=L_i(\xi),\zeta(\eta)=L_j(\eta)$ in (3.13) yields

$$a_{i,j}=b_{i,j},\qquad 0\le i\le N-1,\quad 0\le j\le N-2. \tag{3.15}$$

Using the boundary condition (3.14) and the fact that $L_i(\pm1)=(\pm1)^i$, taking $\phi(\xi)=L_l(\xi)$, $0\le l\le N-1$, gives

$$\begin{cases} b_{l,N-1}+b_{l,N}=\sum\limits_{j=N-1}^{\infty}a_{l,j}, & 0\le l\le N-1,\quad \text{for } \eta=1,\\ b_{l,N-1}-b_{l,N}=\sum\limits_{j=N-1}^{\infty}a_{l,j}(-1)^{j-N+1}, & 0\le l\le N-1,\quad \text{for } \eta=-1, \end{cases} \tag{3.16}$$

then,

$$b_{l,N-1}=\sum_{j=0,j\text{even}}^{\infty}a_{l,N-1+j},\qquad b_{l,N}=\sum_{j=0,j\text{odd}}^{\infty}a_{l,N-1+j}. \tag{3.17}$$

Now utilize (3.15) and (3.17) to estimate $\|\hat{u}_1-\hat{\Pi}_1\hat{u}_1\|_{0,\hat{K}}$:

$$\begin{aligned}\|\hat{u}_1-\hat{\Pi}_1\hat{u}_1\|_{0,\hat{K}}&=\sum_{i=0}^{\infty}\sum_{j=0}^{\infty}\frac{4(a_{ij}-b_{ij})^2}{(2i+1)(2j+1)}\qquad (b_{i,j}=0,\text{ when } i\ge N \text{ or } j\ge N+1)\\ &=4\left(\sum_{i=0}^{N-1}+\sum_{i=N}^{\infty}\right)\left(\sum_{j=0}^{N-2}+\sum_{j=N-1}^{N}+\sum_{j=N+1}^{\infty}\right)\frac{(a_{ij}-b_{ij})^2}{(2i+1)(2j+1)}\\ &=4\sum_{i=0}^{\infty}\sum_{j=N-1}^{N}①\frac{(a_{ij}-b_{ij})^2}{(2i+1)(2j+1)}\\ &\quad+4\left(\sum_{i=0}^{N-1}\sum_{j=N+1}^{\infty}②+\sum_{i=N}^{\infty}\sum_{j=0}^{N-2}③+\sum_{i=N}^{\infty}\sum_{j=N+1}^{\infty}④\right)\frac{a_{ij}^2}{(2i+1)(2j+1)}.\end{aligned}$$

For $s\ge0$, the ② term

$$\begin{aligned}4\sum_{i=0}^{N-1}\sum_{j=N+1}^{\infty}\frac{a_{ij}^2}{(2i+1)(2j+1)}&\le4\sum_{i=0}^{N-1}\sum_{j=N+1}^{\infty}\frac{a_{ij}^2}{(2i+1)(2j+1)}\frac{(1+i^2+j^2)^s}{(1+j^2)^s}\\ &\le\frac{C}{N^{2s}}\|\hat{u}_1\|_{s,\hat{K}}^2,\end{aligned}$$

https://doi.org/10.4208/cicp.230113.140814a Published online by Cambridge University Press

and similarly, the marked term ③

$$4\sum_{i=N}^{\infty}\sum_{j=0}^{N-2}\frac{a_{ij}^2}{(2i+1)(2j+1)}\leq 4\sum_{i=N}^{\infty}\sum_{j=0}^{N-2}\frac{a_{ij}^2}{(2i+1)(2j+1)}\frac{(1+i^2+j^2)^s}{(1+i^2)^s}$$
$$\leq\frac{C}{N^{2s}}\|\hat{u}_1\|_{s,\hat{K}}^2,$$

the ④ term

$$4\sum_{i=N}^{\infty}\sum_{j=N+1}^{\infty}\frac{a_{ij}^2}{(2i+1)(2j+1)}\leq 4\sum_{i=N}^{\infty}\sum_{j=N+1}^{\infty}\frac{a_{ij}^2}{(2i+1)(2j+1)}\frac{(1+i^2+j^2)^s}{(1+N^2+N^2)^s}$$
$$\leq\frac{C}{N^{2s}}\sum_{i=0}^{\infty}\sum_{j=0}^{\infty}\frac{a_{ij}^2(1+i^2+j^2)^s}{(2i+1)(2j+1)}$$
$$\leq\frac{C}{N^{2s}}\|\hat{u}_1\|_{s,\hat{K}}^2.$$

Then in order to estimate the marked term ①, we use (3.17) and let $j=N-1$, obtain

$$A=4\sum_{i=0}^{\infty}\frac{(a_{i,N-1}-b_{i,N-1})^2}{(2i+1)(2N-1)}=4\sum_{i=0}^{\infty}\frac{\left(\sum\limits_{\mathrm{j=1},j\ \mathrm{odd}}^{\infty}a_{i,N+j}\right)^2}{(2i+1)(2N-1)}.\tag{3.18}$$

Now for $s_1>1/2$ and use Cauchy-Schwarz inequality

$$\left(\sum_{\mathrm{j=1},j\ \mathrm{odd}}^{\infty}a_{i,N+j}\right)^2\leq\sum_{j=N+1}^{\infty}a_{ij}^2(1+i^2+j^2)^{s_1}\sum_{j=N+1}^{\infty}(1+i^2+j^2)^{-s_1}$$
$$\leq CN^{-(2s_1-1)}\sum_{j=N+1}^{\infty}a_{ij}^2(1+i^2+j^2)^{s_1}$$
$$\leq CN^{-(2s_1-1)}\sum_{j=N+1}^{\infty}\frac{a_{ij}^2(1+i^2+j^2)^{s_1+\frac{1}{2}}}{(2j+1)},$$

if $s=s_1+\frac{1}{2}>1$, then

$$4\sum_{i=0}^{\infty}\frac{\left(\sum\limits_{\mathrm{j=1},j\ \mathrm{odd}}^{\infty}a_{i,N+j}\right)^2}{(2i+1)(2N-1)}\leq\frac{4}{(2N-1)}\sum_{i=0}^{\infty}\frac{\left(\sum\limits_{j=1,j\ \mathrm{odd}}^{\infty}a_{i,N+j}\right)^2}{(2i+1)}$$
$$\leq CN^{-2s_1}\sum_{i=0}^{\infty}\sum_{j=0}^{\infty}\frac{a_{ij}^2(1+i^2+j^2)^{s_1+1/2}}{(2i+1)(2j+1)}$$
$$\leq CN^{-2s_1}\|\hat{u}_1\|_{s_1+1/2,\hat{K}}^2=CN^{-2(s-1/2)}\|\hat{u}_1\|_{s,\hat{K}}^2.$$

https://doi.org/10.4208/cicp.230113.140814a Published online by Cambridge University Press

Meanwhile for $j=N$ we can have the similar derivation and a similar argument can be used to bound $\|\hat{u}_2-\hat{\Pi}_2\hat{u}_2\|_{0,\hat{K}}$. Therefore we have proved Theorem 3.1. □

Next we prove an *hp*-version estimate for the approximation of the curl of a function. The main results are as follows.

Theorem 3.3. *Let* $\nabla\times\mathbf{u}\in H^r(\Omega)$ *and* $\mathbf{u}\in(H^{r+1}\Omega)^2$ *for* $r>\frac{1}{2}$, *then there is a constant* C *independent of* $\mathbf{u}$ *such that*

$$\|\nabla\times\mathbf{u}-\nabla\times\Pi_N\mathbf{u}\|_{0,\Omega}\leq h^{\min(N,r)}N^{-(r-\frac{1}{2})}\|\nabla\times\mathbf{u}\|_{r,\Omega}. \tag{3.19}$$

In order to prove this theorem, we need to recall Nédélec's divergence-conforming vector elements in $\mathbb{R}^2$. The polynomial space and the degrees of freedom on the reference elements $[-1,1]^2$ are as follows:

$$Q_N^D=\{\mathbf{u}=(\hat{u}_1,\hat{u}_2)\mid \hat{u}_1\in Q_{N,N-1},\ \hat{u}_2\in Q_{N-1,N}\},$$

and

$$\begin{aligned}M_e(\mathbf{u})&=\left\{\int_e\mathbf{u}\cdot\mathbf{n}_e\,q\,\mathrm{d}s,\ q\in Q_{N-1}(e),\right.\\&\qquad\left.\text{for each edge of }\hat{K}\text{and }\mathbf{n}_e\text{ is the unit normal vector of e}\right\},\\M_f(\mathbf{u})&=\left\{\int_f\mathbf{u}\cdot\mathbf{q}\,\mathrm{d}A,\ \mathbf{q}\in Q_{N-2,N-1}\times Q_{N-1,N-2}(f)\right\}.\end{aligned} \tag{3.20}$$

We define an interpolant $\hat{\Pi}_D:(H^r(\hat{K}))^2\to Q_N^D$ for $r>\frac{1}{2}$ satisfying:

$$M_e(\hat{\mathbf{u}}-\hat{\Pi}_D\hat{\mathbf{u}})=M_f(\hat{\mathbf{u}}-\hat{\Pi}_D\hat{\mathbf{u}})=\{0\}.$$

For any $\mathbf{u}(K)\in H(\mathrm{div};K)$, we employ the affine map $\mathbf{u}=\frac{1}{\det(\mathbf{J})}\mathbf{J}\hat{\mathbf{u}}$ and first obtain a *p*-version interpolation estimation on $\hat{K}$.

Theorem 3.4. *Let* $\hat{\mathbf{u}}\in(H^r(\hat{K}))^2$ *for* $r>\frac{1}{2}$, *then there is a constant* C *depending on* $\hat{K}$ *and* r *but not* N *or* $\hat{\mathbf{u}}$ *such that*

$$\|\hat{\mathbf{u}}-\hat{\Pi}_D\hat{\mathbf{u}}\|_{r,\hat{K}}\leq CN^{-(r-\frac{1}{2})}\|\hat{\mathbf{u}}\|_{r,\hat{K}}. \tag{3.21}$$

For the *hp*-version estimation, we also need the following lemma

Lemma 3.2. *Let* $\hat{\mathbf{u}}\in(H^r(\hat{K}))^2$ *and* $\mathbf{u}\in(H^r(K))^2$, $r\geq 0$ *and they are related by the div-conforming transformation. Then*

$$\inf_{\hat{\mathbf{w}}\in(Q_{N-1,N-1})^2}\|\hat{\mathbf{u}}-\hat{\mathbf{w}}\|_{0,\hat{K}}\leq Ch_K^{\min(N,r)}\|\mathbf{u}\|_{r,K}.$$

https://doi.org/10.4208/cicp.230113.140814a Published online by Cambridge University Press

From Theorem 3.4 and Lemma 3.2 we get the *hp*-interpolation result for $H(\mathrm{div};\Omega)$ elements.

Theorem 3.5. *Let* $\mathbf{u}\in(H^r(\Omega))^2$ *for some* $r>\frac{1}{2}$, *then there is a constant* C *independent of* $\mathbf{u}$ *and* N *such that*

$$\|\mathbf{u}-\Pi_D\mathbf{u}\|_{0,\Omega}\leq Ch^{\min(N,r)}N^{-(r-\frac{1}{2})}\|\mathbf{u}\|_{r,\Omega}. \tag{3.22}$$

Proof. This is similar to the proof of Theorem 3.2, by Theorem 3.4 and Lemma 3.2, we can get for any $\hat{\mathbf{w}}\in(Q_{N-1,N-1})^2$

$$\|\hat{\mathbf{u}}-\hat{\Pi}_D\hat{\mathbf{u}}\|_{0,\hat{K}}=\|(I-\hat{\Pi}_D)(\hat{\mathbf{u}}-\hat{\mathbf{w}})\|_{0,\hat{K}}\leq CN^{-(r-\frac{1}{2})}\|\hat{\mathbf{u}}-\hat{\mathbf{w}}\|_{r,\hat{K}},$$
$$\|\mathbf{u}-\Pi_D\mathbf{u}\|_{0,K}\leq C\|\hat{\mathbf{u}}-\hat{\Pi}_D\hat{\mathbf{u}}\|_{0,\hat{K}}\leq Ch^{\min(N,r)}N^{-(r-\frac{1}{2})}\|\mathbf{u}\|_{r,K},$$

summing over all $K\in\Gamma_h$ and noting that $h_K\leq h$, then prove the desired result. □

We now prove Theorem 3.4.

Proof. As in the proof of Theorem 3.1, we only need to prove the result for one component of $\hat{u}_1$. Applying Legendre polynomials, we have

$$(\hat{\Pi}_D\hat{u}_1)=\sum_{i=0}^{N}\sum_{j=0}^{N-1}c_{ij}L_i(\xi)L_j(\eta),$$

and the degrees of freedom (3.20) give

$$\int_{-1}^{1}\int_{-1}^{1}(\hat{u}_1-\hat{\Pi}_D\hat{u}_1)(\xi,\eta)\phi(\xi)\zeta(\eta)d\xi d\eta=0 \qquad \forall\phi\in Q_{N-2},\ \zeta\in Q_{N-1}, \tag{3.23}$$
$$\int_{-1}^{1}(\hat{u}_1-\hat{\Pi}_D\hat{u}_1)(\pm1,\eta)\zeta(\eta)d\eta=0 \qquad \forall\zeta\in Q_{N-1}. \tag{3.24}$$

Taking $\phi(\xi)=L_i(\xi)$, $\zeta(\eta)=L_j(\eta)$ and the orthogonality relation (3.8) in (3.23), we can get

$$a_{ij}=c_{ij}, \qquad \text{for } 0\leq i\leq N-2;\quad 0\leq j\leq N-1. \tag{3.25}$$

Using the choice $\zeta(\eta)=L_\beta(\eta)$, $0\leq\beta\leq N-1$, then

$$c_{N-1,\beta}=\sum_{i=0,i\,\mathrm{even}}^{\infty}a_{i+N-1,\beta}, \qquad c_{N,\beta}=\sum_{i=0,i\,\mathrm{odd}}^{\infty}a_{i+N-1,\beta}.$$

The estimation of $\|\hat{u}_1-\hat{\Pi}_D\hat{u}_1\|_{0,\hat{K}}$ becomes

$$\|\hat{u}_1-\hat{\Pi}_D\hat{u}_1\|_{0,\hat{K}}=\sum_{i=0}^{\infty}\sum_{j=0}^{\infty}\frac{4(a_{ij}-c_{ij})^2}{(2i+1)(2j+1)} \qquad (c_{i,j}=0,\text{when } i\geq N-1 \text{ or } j\geq N)$$
$$=4\left(\sum_{i=0}^{N-2}+\sum_{i=N-1}^{N}+\sum_{i=N+1}^{\infty}\right)\left(\sum_{j=0}^{N-1}+\sum_{j=N}^{\infty}\right)\frac{(a_{ij}-c_{ij})^2}{(2i+1)(2j+1)}$$

https://doi.org/10.4208/cicp.230113.140814a Published online by Cambridge University Press

$$=4\sum_{i=N-1}^{N}\sum_{j=0}^{N}①\frac{(a_{ij}-c_{ij})^2}{(2i+1)(2j+1)}$$
$$+4\left(\sum_{i=0}^{N-2}\sum_{j=N}^{\infty}②+\sum_{i=N+1}^{\infty}\sum_{j=0}^{N-1}②+\sum_{i=N+1}^{\infty}\sum_{j=N}^{\infty}②\right)\frac{a_{ij}^2}{(2i+1)(2j+1)}.$$

The estimation of $\|\hat{u}_1-\hat{\Pi}_D\hat{u}_1\|_{0,\hat{K}}$ turns out to estimate each term on the right-hand side of the above equation. Each of terms marked ② can be estimated in the same way. For example,

$$\begin{aligned}4\sum_{i=0}^{N}\sum_{j=N}^{\infty}\frac{a_{ij}^2}{(2i+1)(2j+1)}&\le 4\sum_{i=0}^{\infty}\sum_{j=N}^{\infty}\frac{a_{ij}^2}{(2i+1)(2j+1)}\frac{(1+i^2+j^2)^r}{(1+N^2)^r}\\&\le\frac{C}{N^{2r}}\sum_{i=0}^{\infty}\sum_{j=0}^{\infty}\frac{a_{ij}^2(1+i^2+j^2)^r}{(2i+1)(2j+1)}\\&\le\frac{C}{N^{2r}}\|\hat{u}_1\|_{r,\hat{K}}^2,\end{aligned}\tag{3.26}$$

for any $r\ge 0$. It now leaves to estimate the term marked ①. Using the similar estimates to (3.18), we obtain

$$4\sum_{i=N-1}^{N}\sum_{j=0}^{\infty}\frac{(a_{ij}-b_{ij})^2}{(2i+1)(2j+1)}\le CN^{-2(r-\frac{1}{2})}\|\hat{u}_1\|_{r,\hat{K}}^2,$$

for any $r>1$. While for the less regular case $\frac{1}{2}<r\le 1$, we need to find another way to estimate the term ①. Inspired by the proof of Theorem 3.1 [21], we consider the trace of $\hat{\mathbf{u}}$ on $\partial\hat{K}$ is well-posed in $\mathbf{L}^2(\partial\hat{K})$, so

$$\int_{-1}^{1}(\hat{u}_1(\pm1,\eta))^2d\eta<\infty,$$

this means that

$$\sum_{j=0}^{\infty}\frac{2}{(2j+1)}\left(\sum_{i=0}^{\infty}a_{ij}L_i(\pm1)\right)^2<\infty,\tag{3.27}$$

then, the term ① has the following estimation

$$\sum_{i=N-1}^{N}\sum_{j=0}^{N-1}\frac{4(a_{ij}-c_{ij})^2}{(2i+1)(2j+1)}=\sum_{j=0}^{N-1}\left(\frac{4(a_{N-1,j}-c_{N-1,j})^2}{(2N-1)(2j+1)}+\frac{4(a_{N,j}-c_{N,j})^2}{(2N+1)(2j+1)}\right)$$
$$\le\frac{4}{(2N-1)}\sum_{j=0}^{N-1}\frac{1}{(2j+1)}\left\{\left(\sum_{i=2,\text{ even}}^{\infty}a_{i+N-1,j}\right)^2+\left(\sum_{i=3,\text{ odd}}^{\infty}a_{i+N-1,j}\right)^2\right\}$$

https://doi.org/10.4208/cicp.230113.140814a Published online by Cambridge University Press

$$\leq\frac{1}{4(2N-1)}\sum_{j=0}^{N-1}\frac{1}{(2j+1)}\left\{\left(\sum_{i=N+1}^{\infty}a_{i,j}+\sum_{i=N+1}^{\infty}(-1)^{i-N-1}a_{i,j}\right)^2\right.$$
$$\left.+\left(\sum_{i=N+1}^{\infty}a_{i,j}-\sum_{i=N+1}^{\infty}(-1)^{i-N-1}a_{i,j}\right)^2\right\}$$
$$\leq\frac{1}{2(2N-1)}\sum_{j=0}^{N-1}\frac{1}{(2j+1)}\left\{\left(\sum_{i=0}^{\infty}a_{i,j}\right)^2+\left(\sum_{i=0}^{\infty}(-1)^i a_{i,j}\right)^2+\left(\sum_{i=0}^{N}a_{i,j}\right)^2+\left(\sum_{i=0}^{N}(-1)^i a_{i,j}\right)^2\right\}.$$

The first two infinite terms can be bounded by the estimation (3.27), finally we can rewrite the formulations

$$\sum_{i=N-1}^{N}\sum_{j=0}^{N-1}\frac{4(a_{ij}-c_{ij})^2}{(2i+1)(2j+1)}$$
$$\leq\frac{1}{2(2N-1)}\left\{\|\hat{u}_1\|_{0,\partial\hat{K}}+\sum_{j=0}^{N-1}\sum_{i=0}^{N}\frac{a_{ij}^2(1+i^2+j^2)^r}{(2i+1)(2j+1)}\times\sum_{j=0}^{N-1}\sum_{i=0}^{N}\frac{(2i+1)}{(1+i^2+j^2)^r}\right\}$$
$$\leq C(N^{-1}\|\hat{u}_1\|_{0,\partial\hat{K}}+N^{-2(r-1/2)}\|\hat{u}_1\|_{r,\hat{K}})$$
$$\leq CN^{-2(r-1/2)}\|\hat{u}_1\|_{r,\hat{K}},$$

for any $\frac{1}{2}<r\leq 1$. Therefore, combining the above estimates and obtaining the similar analysis for $\hat{\mathbf{u}}_2$ prove the theorem. □

Applying Theorem 3.4 we can easily prove Theorem 3.3.

Proof. Suppose $\mathbf{u}$ is sufficiently smooth and $\Pi\mathbf{u}$ is well-defined, we can obtain that

$$\nabla\times\Pi\mathbf{u}=\Pi_D\nabla\times\mathbf{u},$$

then,

$$\|\nabla\times\mathbf{u}-\nabla\times\Pi\mathbf{u}\|_{0,\Omega}=\|\nabla\times(\mathbf{u}-\Pi\mathbf{u})\|_{0,\Omega}=\|(I-\Pi_D)(\nabla\times\mathbf{u})\|_{0,\Omega},$$

the result immediately comes by Theorem 3.4. □

Now we begin to prove the assumptions. Let Ω be the convex polyhedron that can be meshed using quadrilateral elements that are affine equivalent to the reference element. The mesh Γ_h is regular and quasi uniform. Then we prove the validity of ellipticity on the discrete kernel.

Lemma 3.3. *There exists a constant C not depending on h and N such that for all $\mathbf{v}_h\in\mathbb{K}_h$ it holds*

$$\|\mathbf{v}_h\|_0\leq C\|\nabla\times\mathbf{v}_h\|_0. \tag{3.28}$$

https://doi.org/10.4208/cicp.230113.140814a Published online by Cambridge University Press

Proof. Refer to Theorem 4.7 of [23], for $\mathbf{v}_h \in \mathbb{K}_h$ use its Helmholtz decompositions

$$\mathbf{v}_h = \begin{cases} \mathbf{z} + \nabla q, & z \in \mathbb{K}, \\ \mathbf{z}_h + \nabla q_h, & z_h \in \mathbb{K}_h, \end{cases}$$

and modify the Lemma 4.5 of [23] to hp-version estimates and use the interpolation error estimates Theorem 3.2, we can get

$$\|\mathbf{z} - \mathbf{z}_h\|_0 \leq C h^{\min(N,s)} N^{-(s-\frac{1}{2})} \|\nabla \times \mathbf{v}_h\|_0, \tag{3.29}$$

then,

$$\begin{aligned} (\mathbf{v}_h, \mathbf{v}_h)_0 &= (\mathbf{v}_h, \mathbf{z}_h + \nabla q_h)_0 = (\mathbf{v}_h, \mathbf{z}_h)_0 \\ &= (\mathbf{v}_h, \mathbf{z}_h - \mathbf{z})_0 + (\mathbf{v}_h, \mathbf{z})_0 \\ &\leq \|\mathbf{v}_h\|_0 (\|\mathbf{z}_h - \mathbf{z}_0\| + \|\mathbf{z}\|_0), \end{aligned}$$

using the above inequality and Poincaré-Friedrichs-type inequality (see Corollary 4.4 of [23]) yields the desired estimate. □

Let us now prove Assumption 2.3.

Lemma 3.4. *For all $\mathbf{v}_h \in \mathbb{K}_h$ there exists $\mathbf{v} \in \mathbb{K}_h$ such that*

$$\|\mathbf{v}_h - \mathbf{v}\|_0 \leq C h^{\min(N,s)} N^{-(s-\frac{1}{2})} \|\mathbf{v}_h\|_{\text{curl}}.$$

Proof. For $\mathbf{v}_h \in \mathbb{K}_h$, according to the proof of the previous lemma we can get

$$\|\mathbf{v} - \mathbf{v}_h\|_0 \leq C h^{\min(N,s)} N^{-(s-\frac{1}{2})} \|\nabla \times \mathbf{v}_h\|_0.$$

This completes the proof. □

We finish the proof of Assumption 2.3 by

$$\sup_{\mathbf{v}_h \in \mathbf{K}_h} \frac{b(p, \mathbf{v}_h)}{\|\mathbf{v}_h\|_{\text{curl}}} = \sup_{\mathbf{v}_h \in \mathbf{K}_h} \frac{b(p, \mathbf{v}_h - \mathbf{v})}{\|\mathbf{v}_h\|_{\text{curl}}} \leq C h^{\min(N,s)} N^{-(s-\frac{1}{2})} \|p\|_1. \tag{3.30}$$

Proof of Assumption 2.4:

Lemma 3.5. *For all $\mathbf{u} \in H(curl;\Omega)$ with $\mathbf{u} \in \mathbb{K}$ and satisfying regularity Assumption* 2.1 *there is an element $\mathbf{u}^I \in \mathbb{K}_h$ satisfying*

$$\|\mathbf{u} - \mathbf{u}^I\|_{\text{curl}} \leq C h^{t_1} N^{-t_2} (\|\mathbf{u}\|_s + \|\nabla \times \mathbf{v}_h\|_r), \quad \textit{with} \;\; t_1 = \min(N,s,r), \;\; t_2 = \min\left(s - \frac{1}{2}, r\right).$$

https://doi.org/10.4208/cicp.230113.140814a Published online by Cambridge University Press

Proof. Applying Lemma 9 in [11], we can obtain

$$\|\mathbf{u}-\mathbf{u}^I\|_{\text{curl}} \leq C \inf_{\mathbf{v}_h \in V_h} \|\mathbf{u}-\mathbf{u}_h\|_{\text{curl}},$$

then using Theorems 3.2 and 3.3, the error estimate becomes

$$\begin{aligned}\|\mathbf{u}-\Pi\mathbf{u}\|_{\text{curl}} &= \|\mathbf{u}-\Pi\mathbf{u}\|_0 + \|\nabla\times\mathbf{u}-\nabla\times\Pi\mathbf{u}\|_0 \\ &= Ch^{\min(N,s)}N^{-(s-\frac{1}{2})}\|\mathbf{u}\|_s + Ch^{\min(N,r)}N^{(-r)}\|\nabla\times\mathbf{u}\|_r \\ &= Ch^{t_1}N^{-t_2}(\|\mathbf{u}\|_s + \|\nabla\times\mathbf{u}\|_r).\end{aligned}$$

This completes the proof. □

Finally, as the consequence of the results of [12], we have the following theorem:

Theorem 3.6. *There exists a constant C such that for all $\mathbf{f}\in\mathbf{L}^2(\Omega)$ it holds*

$$\|T\mathbf{f}-T_h\mathbf{f}\|_{\text{curl}} \leq Ch^{t_1}N^{-t_2}\|\mathbf{f}\|_0, \tag{3.31}$$

where t_1,t_2 is the same as in Lemma 3.5*, and s and r are given in Assumption* 2.1*.*

Proof. Let $\mathbf{f}\in\mathbf{L}^2(\Omega)$ and consider the solutions $(\mathbf{u},p)$ of (2.7) and the discrete solutions $(\mathbf{u}_h,p_h)$ of (2.11). In order to estimate the error $\|T\mathbf{f}-T_h\mathbf{f}\|_{\text{curl}} = \|\mathbf{u}-\mathbf{u}_h\|_{\text{curl}}$, we need to bound the error $\|\mathbf{u}^I-\mathbf{u}_h\|_{\text{curl}}$, From the ellipticity in the kernel of a we obtain

$$\begin{aligned}\alpha\|\mathbf{u}^I-\mathbf{u}_h\|_{\text{curl}} &\leq a(\mathbf{u}^I-\mathbf{u}_h,\mathbf{u}^I-\mathbf{u}_h) \\ &= a(\mathbf{u}^I-\mathbf{u},\mathbf{u}^I-\mathbf{u}_h) + a(\mathbf{u}-\mathbf{u}_h,\mathbf{u}^I-\mathbf{u}_h) \\ &= a(\mathbf{u}^I-\mathbf{u},\mathbf{u}^I-\mathbf{u}_h) - b(\mathbf{u}^I-\mathbf{u}_h,p-p_h) \\ &\leq C\|\mathbf{u}^I-\mathbf{u}\|_{\text{curl}}\|\mathbf{u}^I-\mathbf{u}_h\|_{\text{curl}} + |b(\mathbf{u}^I-\mathbf{u}_h,p-p_h)| \\ &\leq \left(C\|\mathbf{u}^I-\mathbf{u}\|_{\text{curl}} + \sup_{\mathbf{v}_h\in\mathbb{K}_h}\frac{b(\mathbf{v}_h,p)}{\|\mathbf{v}_h\|_{\text{curl}}}\right)\|\mathbf{u}^I-\mathbf{u}_h\|_{\text{curl}}.\end{aligned}$$

Using the strong approximability of $\mathbf{H}_0(\text{curl},\Omega)$ and the weak approximability of $H_0^1(\Omega)$ gives the required estimates. □

3.3 Discretized eigenvalue problem

Substituting (3.6) into the variational formulas (2.9) and (2.10), and exploiting the covariant mapping (3.5), we discretize the equation for SEM into a generalized eigenvalue matrix equation

$$\mathbf{Se} = \lambda\mathbf{Me}, \tag{3.32}$$

https://doi.org/10.4208/cicp.230113.140814a Published online by Cambridge University Press

where **e** is the column vector of the electric field along the edges, and **S** is the stiffness matrix and **M** is the mass matrix. Similarly, the discretized eigenvalue equation for the mixed SEM (2.10) is denoted as

$$\begin{cases} \mathbf{Se}+\mathbf{Ky}=\lambda\mathbf{Me}, \\ \mathbf{K}^{\mathrm{T}}\mathbf{e}=0, \end{cases} \tag{3.33}$$

where matrix **K** is the weak analogue of the divergence equation and **y** is the column vector of p_h at all of the nodal points. The stiffness matrix, mass matrix and matrix **K** are the assembling of the elemental matrices from the N_e elements in the global mesh

$$\mathbf{S}=\sum_{e=1}^{N_e}\mathbf{S}^{(e)}, \quad \mathbf{M}=\sum_{e=1}^{N_e}\mathbf{M}^{(e)}, \quad \mathbf{K}=\sum_{e=1}^{N_e}\mathbf{K}^{(e)}. \tag{3.34}$$

The elemental matrices of the eth element $\mathbf{S}^{(e)}$, $\mathbf{M}^{(e)}$ and $\mathbf{K}^{(e)}$ are

$$\begin{aligned} \mathbf{S}_{ji}^{(e)} &= \int_K \mu_r^{-1}\nabla\times\mathbf{\Phi}_i\cdot\nabla\times\mathbf{\Phi}_j\mathrm{d}x\mathrm{d}y=\int_{-1}^{1}\int_{-1}^{1}\mu_r^{-1}\frac{1}{|\mathbf{J}|}\hat{\nabla}\times\hat{\mathbf{\Phi}}_i\cdot\hat{\nabla}\times\hat{\mathbf{\Phi}}_j\mathrm{d}\xi\mathrm{d}\eta, \\ \mathbf{M}_{ji}^{(e)} &= \int_K \epsilon_r\mathbf{\Phi}_i\cdot\mathbf{\Phi}_j\mathrm{d}x\mathrm{d}y=\int_{-1}^{1}\int_{-1}^{1}\epsilon_r\hat{\mathbf{\Phi}}_i^T\mathbf{J}^{-T}\mathbf{J}^{-1}\hat{\mathbf{\Phi}}_j|\mathbf{J}|\mathrm{d}\xi\mathrm{d}\eta, \\ \mathbf{K}_{ji}^{(e)} &= \int_K \epsilon_r\nabla\Psi_i\cdot\mathbf{\Phi}_j\mathrm{d}x\mathrm{d}y=\int_{-1}^{1}\int_{-1}^{1}\epsilon_r\hat{\nabla}\hat{\Psi}_i^T\mathbf{J}^{-T}\mathbf{J}^{-1}\hat{\mathbf{\Phi}}_j|\mathbf{J}|\mathrm{d}\xi\mathrm{d}\eta, \end{aligned}$$

where the integration region K is the eth element.

In order to solve the eigenvalue problem (3.33) we employ the technique introduced by Bespalov [24] and consider the eigenvalue problem

$$\mathbf{Se}+\mathbf{KHK}^{\mathrm{T}}\mathbf{e}=\tilde{\lambda}\mathbf{Me}. \tag{3.35}$$

If the positive definite matrix **H** is chosen properly, the zero eigenvalues are shifted inside the spectrum of **S** relative to **M** and do not disturb the computation [17]. Bespalov suggests to select **H** as a multiple of the identity. In consideration of the dimensional homogeneity on both sides of equation (3.35), where $\|\mathbf{S}\|$ grows in accordance with $(\frac{1}{h})^2$ of the dimension, but $\|\mathbf{M}\|$ and $\|\mathbf{K}\|$ don't change. Therefore, **H** is chosen to be $\alpha\mathbf{I}$ with $\alpha=(\frac{10}{h})^2$, where h is the smallest length of two interplant points of the mesh Ω. The solution to this eigenvalue problem is obtained with the help of MATLAB platform.

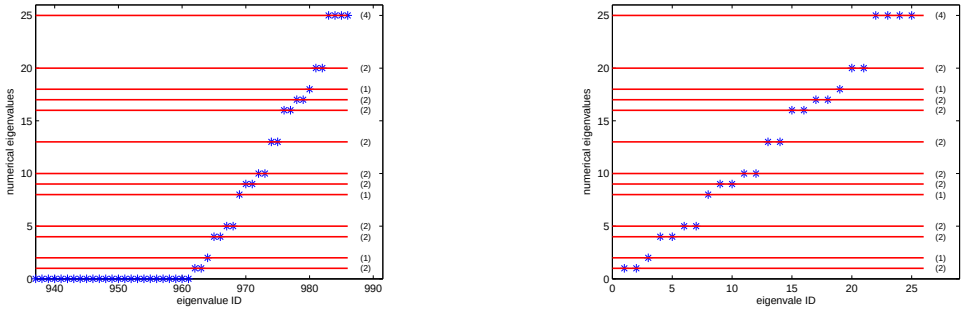
4 Numerical results

In this section, we consider a series of numerical experiments on the mixed spectral element method to verify its higher accuracy and efficiency. They confirm that the method is free of all spurious modes, has exponential accuracy and is advantageous in the CPU time and memory.

https://doi.org/10.4208/cicp.230113.140814a Published online by Cambridge University Press

4.1 Square cavity

We consider a cavity defined by a square domain $\Omega=[0,\pi]^2$. The exact Maxwell eigenvalues on this domain are given by $\lambda=m^2+n^2$, where $m,n=0,1,2,3,4,\cdots$ and $m^2+n^2\neq 0$ [25]. The comparison between (2.9) and (2.10) in Fig. 3 shows that the mixed SEM can suppress all spurious zero and nonzero eigenvalues, while the number of spurious zero eigenvalues of method (2.9) is equal to the number of the internal nodes of the SEM mesh. The first 25 nonzero eigenvalues are shown in Fig. 3. As the order of basis functions is $N=4$ and number of divisions in x and y directions $Ne=\pi/h=8$, there are 961 internal vertices in the uniform mesh, Thus, employing (2.9) yields 961 spurious zero eigenvalues, as shown in Fig. 3(a). On the other hand, employing (2.10) yields no spurious eigenvalues in Fig. 3(b).



(a) (b)

Figure 3: The eigenvalue problem of a homogeneous square cavity. (a) 961 zero eigenvalues appear in the regular SEM on a uniform mesh with $Ne=8$ and $N=4$. Here the analytical solutions of the eigenvalues are shown by horizontal lines with (1) or (2) indicating the multiplicity of the eigenvalues. (b) The mixed SEM is free of spurious zero eigenvalues.

Furthermore, we plot the first 7 numerical eigenvalues from mixed SEM versus the order of basis functions in Fig. 4, from which we can see the spectral accuracy property for the mixed SEM, i.e., the error decreases exponentially as N increases (the error is defined as $|\lambda-\tilde{\lambda}|/\tilde{\lambda}$ where $\tilde{\lambda}$ is the analytical eigenvalues or the reference values), and the 7^{th} eigenvalue converges more slowly than the 1^{st} solution because of its higher frequency.

For this square computational domain the exact solution for the eigenvector is quite smooth and can be written as

$$\mathbf{u}=\begin{bmatrix} \frac{n}{m^2+n^2}\cos(mx)\sin(ny) \\ -\frac{m}{m^2+n^2}\sin(mx)\cos(ny) \end{bmatrix}.$$

According to the estimate of Theorem 3.6, we can see that for the fixed order of basis functions N the eigenvector convergence rate with the mesh size h is given by:

$$\|\mathbf{u}-\mathbf{u}_h\|_{\mathrm{L}^2(\Omega)}\leq Ch^N\|\mathbf{u}\|_{\mathrm{L}^2(\Omega)}. \tag{4.1}$$

https://doi.org/10.4208/cicp.230113.140814a Published online by Cambridge University Press

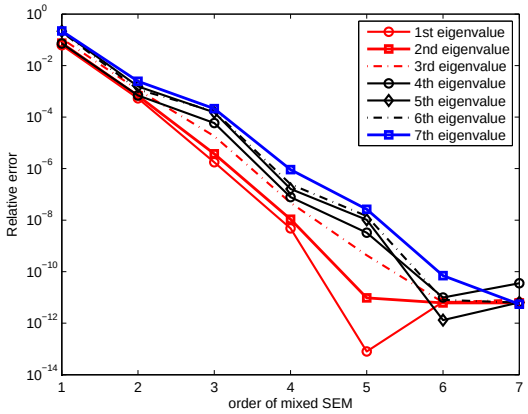


Figure 4: Relative error versus the order of the mixed SEM basis functions in a semilog scale plot.

For the simplest case, the convergence results of TE_{11} mode with $N=1$ is tabulated in Table 1 to confirm the estimation of (4.1).

It is known that the convergence rate of numerical eigenvalues doubles the order of basis functions, thus, with the first order GLL basis functions the convergence rate of approximate eigenvalues should be second order. To save space, only the first 5 numerical eigenvalues and their convergence rates are included in Table 2 to verify the convergence rate.

Table 1: Eigenvector convergence of the mixed SEM on the square $[0,\pi]^2$ with $N=1$ on uniform meshes.

$Ne=\frac{\pi}{h}$	$\frac{\|\mathbf{u}-\mathbf{u}_h\|_{L^2(\Omega)}}{\|\mathbf{u}\|_{L^2(\Omega)}}$	order
2	0.504342	
4	0.220773	1.19
8	0.104331	1.08
16	0.051321	1.02
32	0.025552	1.01

Table 2: The eigenvalue convergence rate of the mixed SEM for the square cavity with $N=1$.

$Ne=\frac{\pi}{h}$	1^{st}	2^{nd}	3^{rd}	4^{th}	5^{th}
4	1.052	1.052	2.105	4.863	4.863
8	1.013(2.02)	1.013(2.02)	2.026(2.02)	4.210(2.04)	4.210(2.04)
16	1.003(2.01)	1.003(2.01)	2.006(2.01)	4.052(2.02)	4.052(2.02)
32	1.001(2.00)	1.001(2.00)	2.002(2.00)	4.013(2.01)	4.013(2.01)
64	1.000(2.00)	1.000(2.00)	2.000(2.00)	4.003(2.00)	4.003(2.00)
Exact	1	1	2	4	4

https://doi.org/10.4208/cicp.230113.140814a Published online by Cambridge University Press

4.2 L-shape cavity

The L-shape cavity $\Omega=[-1,1]^2\backslash\{[0,1]\times[-1,0]\}$ is studied next based on Dauge's benchmark examples for the Maxwell eigenproblem [26]. The first 5 smallest eigenvalues are 1.4756218, 3.5340314, 9.8696044, 9.8696044, 11.3894794, respectively. It is also known that the 1^{st} and 5^{th} eigenfunctions have a strong unbounded singularity, the 2^{nd} one belongs to $\mathbf{H}^1(\Omega)$, and the 3^{rd} and the 4^{th} ones are analytic. Specifically, the first eigenfunction around the $(0,0)$ is proportional to $\rho^{-\frac{1}{3}}$, where ρ is the radius in polar coordinate. To verify the spectral accuracy on this L-shape cavity, we show the first 5 smallest numerical eigenvalues from the mixed SEM versus the order of basis functions in Fig. 5. Due to the singularity of eigenfunctions the mixed SEM has lost its spectral accuracy. Now it is more efficient to get higher accuracy eigenvalues through using singular basis functions as mentioned in [27–29] or refining mesh around the singular point $(0,0)$. Fig. 6 gives the field distribution of the first and second eigenfunctions, respectively. We can see clearly from Fig. 6(a) that the electric field around $(0,0)$ is pretty large.

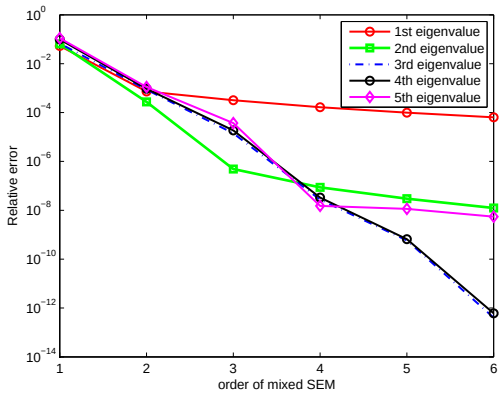
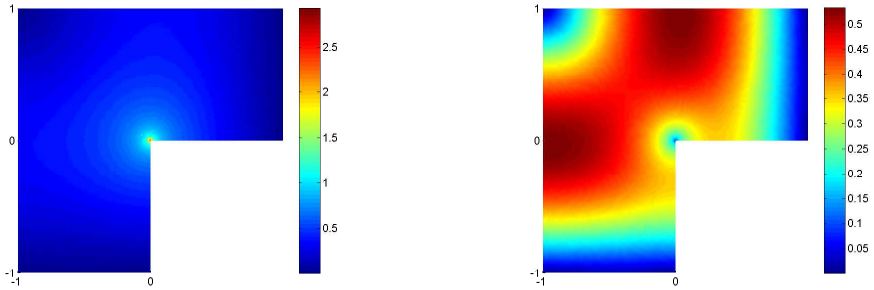


Figure 5: Relative error versus the order of the mixed SEM basis functions in a semilog plot on an L-shape cavity.



(a) (b)

Figure 6: Field distribution of norm($\mathbf{E}$) in the L-shape cavity for the first (a) and second (b) singular eigenvectors with $N=3$.

https://doi.org/10.4208/cicp.230113.140814a Published online by Cambridge University Press

Table 3: First five lowest eigenvalues of the L-shape cavity computed by the SEM and mixed SEM with N=3.

Mode	Ref. [26]	SEM		Mixed SEM	
No.		λ	Error	λ	Error
1	1.4756	0		1.4752	3.20E-04
2	3.5340	0		3.5340	4.86E-07
3	9.8696	0		9.8697	1.41E-05
4	9.8696	1.4752	3.20E-04	9.8698	1.86E-05
5	11.3895	3.5340	4.86E-07	11.3899	3.72E-05

For many engineering applications, one may only need to know a few smallest eigenvalues, thus the mixed SEM has the tremendous advantages in the CPU time requirement in eigenvalue solver part due to the elimination of spurious zero eigenvalues. In fact, Table 3 shows the first five lowest eigenvalues of the L-shape cavity computed by the SEM and mixed SEM with $N=3$ and the DoF=1,464. The initial eigenvalue for the conventional SEM is chosen as 2. We obtain that the proposed mixed SEM can completely suppress the appearance of zero eigenvalues as expected and its costs 0.30 s CPU time in this eigensolver part, whereas the classical SEM has three zero eigenvalues and costs 1.34 s CPU time, which is about four times more expensive in comparison with the mixed SEM, clearly illustrating the higher efficiency of our proposed method.

4.3 Inhomogeneous cavity

We also calculate Maxwell eigenvalues with an inhomogeneous medium on the domain $[-1,1]^2$ from Dauge's benchmark examples for the Maxwell eigenvalue problem [26]. The cavity consists of four squares, where the upper right and lower left squares are filled with material 1 with $\epsilon_r=0.5$, $\mu_r=1$, while the other two squares are vacuum (material 2) with $\epsilon_r=1$, $\mu_r=1$ as shown in Fig. 7.

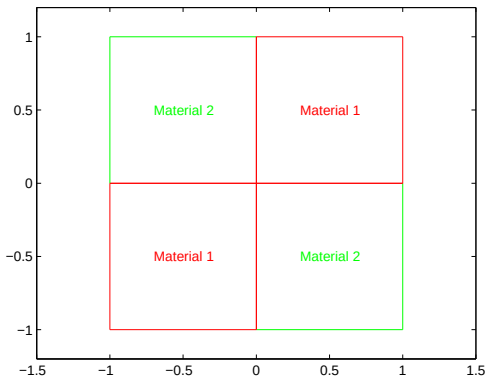


Figure 7: Inhomogeneous computational domain $[-1,1]^2$ with four squares.

https://doi.org/10.4208/cicp.230113.140814a Published online by Cambridge University Press

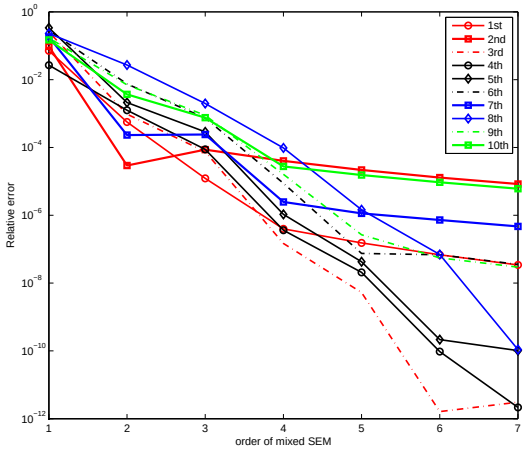


Figure 8: Relative error versus the order of the mixed SEM basis functions in a semilog plot on the inhomogeneous cavity in Fig. 7.

We plot the first 10 numerical eigenvalues from the mixed SEM versus the order of basis functions in Fig. 8. Similar to the singular L-shape eigenvalues, the mixed SEM cannot preserve its spectral accuracy for the eigenvectors with singularities, but for the first 5 smallest eigenvalue, Table 4 shows relative errors to reach an accuracy better than 0.01%, where the sixth-order basis functions are used.

Table 4: Relative error of the first 5 smallest eigenvalue to get an error smaller than 0.01 % for the inhomogeneous cavity in Fig. 7 with $N=6$.

Analytic $[m^{-2}]$	Mixed SEM	Error(%)
3.31754876	3.31754854	6.82E-06
3.36632416	3.36628055	1.30E-03
6.18638956	6.18638956	1.65E-10
13.92632333	13.92632333	9.53E-09
15.08299096	15.08299096	2.14E-08

4.4 Coaxial cavity

Here we considered a coaxial cavity with inner radius a, outer radius b, and dielectric constant ϵ_r inside the coaxial cavity. It is known that the smallest Maxwell eigenvalue on this domain is 0 with multiplicity one. The eigenvalue λ is determined by

$$\mathbf{J}'_m(\lambda a)\mathbf{Y}'_m(\lambda b)-\mathbf{J}'_m(\lambda b)\mathbf{Y}'_m(\lambda a)=0,$$

https://doi.org/10.4208/cicp.230113.140814a Published online by Cambridge University Press

where the prime represents the derivative with the argument of the functions, $\mathbf{J}_m(\lambda a)$ and $\mathbf{Y}_m(\lambda b)$ are the m-th order Bessel functions of first and second kinds, are given by

$$\mathbf{J}_m(\lambda a)=\sum_{n=0}^{\infty}\frac{(-1)^n(\lambda a)^{m+2n}}{n!(n+m)!2^{m+2n}},$$
$$\mathbf{Y}_n(\lambda a)=\frac{\cos(n\pi)\mathbf{J}_n(\lambda a)-\mathbf{J}_{-n}(\lambda a)}{\sin(n\pi)},$$

respectively. The coaxial cavity is divided into a number of non-overlapping curvilinear quadrilateral elements conformal to the geometry, as shown in Fig. 9, and analytic mapping between the reference element and real physical element is applied to increase the accuracy. A curved element in the physical space can be written in terms of the reference coordinates as $x=x(\xi,\eta)$, $y=y(\xi,\eta)$ after a curvilinear mapping between the real physical space (x,y) and reference space (ξ,η). Here the 2D mapping $x(\xi,\eta)$ and $y(\xi,\eta)$ can be expressed by functions of the corresponding four boundary curves and four vertices of the element. For example, $x(\xi,\eta)$ can be constituted by the four boundary curves of one element $x(\xi,-1)$, $x(\xi,1)$, $x(-1,\eta)$, $x(1,\eta)$ and four x coordinates of vertices. These boundary curves could be straight lines or curves depending on the geometry, and can be given analytically or interpolating some controlling points on the curved element. For the circular arc the interface is given by $x=r\cos(\theta\eta)$, where r is the radius (can be equal to a or b) and θ is the angular parameter. Then the 2D curvilinear mapping expressions is

$$x(\xi,\eta)=\frac{1-\eta}{2}x(\xi,-1)+\frac{1+\eta}{2}x(\xi,1)+\frac{1-\xi}{2}x(-1,\eta)+\frac{1+\xi}{2}x(1,\eta)-\left\{\frac{1-\xi}{2}\frac{1-\eta}{2}x(-1,-1)\right.$$
$$\left.+\frac{1+\xi}{2}\frac{1-\eta}{2}x(1,-1)+\frac{1-\xi}{2}\frac{1+\eta}{2}x(-1,1)+\frac{1+\xi}{2}\frac{1+\eta}{2}x(1,1)\right\}.$$

The mapping functions for $y(\xi,\eta)$ is similar, while Fig. 9 illustrates the physical mesh and nodal points in the real place with $N=5$.

To further understand the accuracy of the mixed SEM, its numerical convergence behavior is also examined by comparing the eigenvalue of mixed SEM results with the orders of basis function. We obtained the first 10 smallest nonzero eigenvalues from the mixed SEM with the inner radius $a=1$, outer radius $b=2$ and dielectric constant $\epsilon_r=1$. Fig. 10 shows the average relative error of the smallest 10 eigenvalues, relative error of the second and the tenth eigenvalue versus the mixed SEM order. The convergence curves are nearly straight lines in this semilog plot, also illustrating the spectral accuracy property for the mixed SEM. Besides the higher accuracy of nonzero eigenvalues, the mixed SEM can successfully capture the zero eigenvalue. The eigenvector and the field distribution corresponding to the first zero eigenvalue from the mixed SEM is shown in Fig. 11, which is difficult to obtain from the conventional SEM and COMSOL (a commercial software package) eigenfrequency solver due to the presence of spurious zero eigenvalues.

https://doi.org/10.4208/cicp.230113.140814a Published online by Cambridge University Press

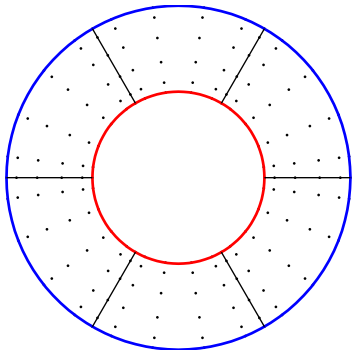


Figure 9: The mixed SEM mesh and nodal points in the real physical place with $N=5$ for a coaxial cavity.

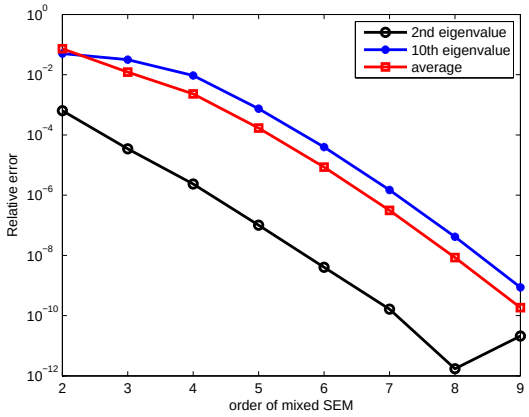
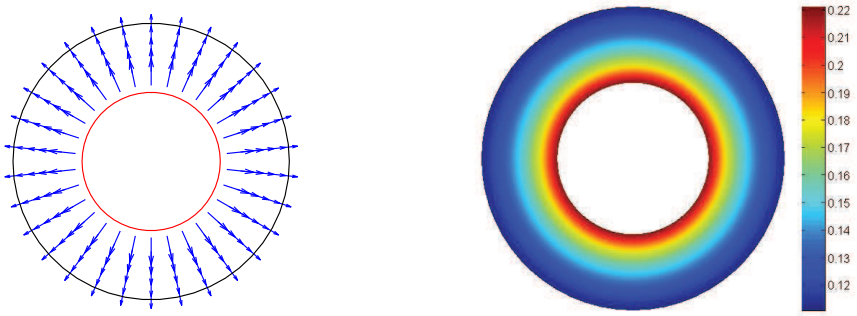


Figure 10: The average relative error of the smallest 10 eigenvalues, relative error of the first and the tenth eigenvalue versus the mixed SEM order for the coaxial cavity in Fig. 9.



(a) (b)

Figure 11: The corresponding eigenvector and field distribution of norm($\mathbf{E}$) of the first eigenvalue zero with $N=5$ for the coaxial cavity in Fig. 9.

https://doi.org/10.4208/cicp.230113.140814a Published online by Cambridge University Press

Fig. 11(b) is the field distribution of norm $(\mathbf{E})$ in this coaxial cavity, which illustrates that the electric field concentrates along the inner PEC boundary.

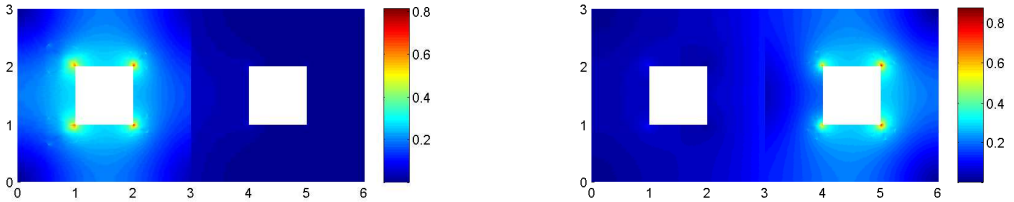
Moreover, in order to demonstrate that the mixed SEM has well satisfied the divergence-free condition, Table 5 presents the first three eigenvalues calculated by the mixed SEM with $N=3$ and the DoF$=90$. Here the measure $\mathrm{Div}(\mathbf{e})$ and $\mathrm{Curl}(\mathbf{e})$ is the numerical value of the divergence and curl of the corresponding eigenvector, which is defined as $\mathrm{Div}(\mathbf{e})=\|\mathbf{Ke}\|$, $\mathrm{Curl}(\mathbf{e})=\|\mathbf{Se}\|$, respectively. We can clearly see that all the eigenvectors computed by the mixed SEM is divergence-free, and the property of the eigenvector associating with the physical zero eigenvalue having no irrotational component is also verified from Table 5.

Table 5: First five lowest eigenvalues of the coaxial cavity in Fig. 9 computed by the mixed SEM with N=3.

Analy.	Mixed SEM	Error	$\mathrm{Div}(\mathbf{e})$	$\mathrm{Curl}(\mathbf{e})$
0	4E-14		2.98E-16	5.16E-16
0.4587	0.4587	3.45E-5	4.04E-16	0.4892
0.4587	0.4587	3.45E-5	4.72E-16	0.4892
1.7972	1.7983	6.49E-4	6.62E-16	1.9174
1.7972	1.7983	6.49E-4	4.66E-16	1.9174

4.5 A dual-inner-conductor cavity

For the last example, we show a dual-inner-conductor cavity with two different media. Suppose $\Omega_1=\{[0,3]^2\setminus[1,2]^2\}$ and $\Omega_2=\{[3,6]\times[1,3]\setminus[4,5]\times[1,2]\}$, the computational domain is $\Omega=\Omega_1\cup\Omega_2$. Suppose Ω_1 is filled with air and domain Ω_2 with $\epsilon_r=3$, $\mu_r=1$. Since there are two inner PEC boundaries in this cavity, it has two zero eigenvalues. For the mixed SEM, it can successfully capture these two physical zero eigenvalues and the numerical values are exactly equal to zero (up to machine precision). Fig. 12 shows the field distribution of norm $(\mathbf{E})$ for the two zero eigenvalues with the order of basis functions $N=3$. From the field distribution we can see the corresponding eigenvectors are singular and the energy almost concentrates at the four inner corners.



(a) (b)

Figure 12: Field distribution of norm$(\mathbf{E})$ in the dual-inner-conductor cavity for the first and second zero eigenvalues with $N=3$.

https://doi.org/10.4208/cicp.230113.140814a Published online by Cambridge University Press

5 Conclusion

A mixed spectral element method (mixed SEM), is investigated to solve the 2D vector Maxwell TEz eigenvalue problem, and an abstract analysis of the exponential convergence of the mixed SEM is presented, which fully confirm the convergence of our method. Gauss-Lobatto-Legendre polynomials are used to construct the higher order curl-conforming edge-based and node-based basis functions. Compared to the conventional higher order SEM, the mixed SEM can successfully eliminate all spurious modes and has spectral accuracy with the error decreasing exponentially with the order of basis functions for analytic eigenvectors. All the numerical examples demonstrate that the mixed SEM is an efficient alternative method for solving the 2D vector Maxwell eigenvalue problem. Future research will focus on 3D Maxwell eigenvalue problems, and improve the spectral accuracy for singular eigenvectors.

Acknowledgments

We would also like to thank Dr. Yanmin Zhao, Mr. Qiang Ren and other research group members for helpful discussions. The research work in this paper was carried out while the first author was visiting Department of Electrical and Computer Engineering, Duke University under the support of Academy of Mathematics and Systems Science, Chinese Academy of Sciences. The research is also partially supported by supported by National Natural Science Foundation of China (Grant Nos. 11371357, 60931002, 41390453, and 61301008), and by Fujian Province Natural Science Foundation (Grant No. 2013J05060).

References

[1] P. Silvester, Finite element solution of homogeneous waveguide problems, Alta Frequenza., 38 (1969), 313-317.
[2] Z. J. Cendes, D. Hudak, J. F. Lee, and D. K Sun, Development of New Methods for Predicting the Bistatic Electromagnetic Scattering from Absorbing Shapes, RADC Final Report, Hansom Air Force Base, MA, 1986.
[3] B. M. A. Rahman, J. B. Davies, Penalty Function Improvement of Waveguide Solution by Finite Elements, IEEE Trans. Microw. Theory Tech., 32 (1984), 922-928.
[4] J. R. Winkler and J. B. Davies, Elimination of spurious modes in finite element analysis, J. Comput. Phys., 56 (1984), 1-14.
[5] A. J. Kobelansky and J. P. Webb, Eliminating spurious modes in finite-element waveguide problems by using divergence-free fields, Electron. Lett., 22 (1986), 569-570.
[6] D. Sun, J. Manges, X. Yuan, Z. Cendes Spurious Modes in Finite Element Methods, IEEE Trans. Microw. Theory Tech., 37 (1995), 12-24.
[7] J. C. Nédélec, Mixed finite elements in R^3, Numer. Mathem., 35 (1980), 315-341.
[8] J. C. Nédélec, A New Family of Mixed Finite Elements in R^3, Numer. Mathem., 50 (1986), 57-81.

https://doi.org/10.4208/cicp.230113.140814a Published online by Cambridge University Press

[9] G. Mur, Edge Elements, their advantages and their disadvantages, IEEE Trans. Magn., 30 (1994), 3552-3557.
[10] D. Boffi, Finite element approximation of eigenvalue problems, Acta Numerica., 19 (2010), 1-120.
[11] D. Boffi, M. Conforti, and L. Gastaldi, Modified edge finite elements for photonic crystals. Numer. Mathem., 105 (2006), 249-266.
[12] D. Boffi, F. Brezzi, L. Gastaldi, On the convergence of eigenvalues for mixed formulations. Ann. Sc. Norm. Sup. Pisa Cl. Sci., 25 (1997), 131C154.
[13] Hiptmair, R. and P.D. Ledger, Computation of resonant modes for axisymmetric Maxwell cavities using hp-version edge finite elements. Int. J. Numer. Meth. Engng, 62 (2005), 1652-1676.
[14] F. Kikuchi, Mixed and penalty formulations for finite element analysis of an eigenvalue problem in electromagnetism, Comput. Methods Appl. Mech. Engrg., 64 (1987), 509-521.
[15] S. C. Brenner, F. Li, L. Sung, Nonconforming Maxwell Eigensolvers, J. Sci. Comput., 40 (2009), 51-85.
[16] P. Monk, Finite element methods for Maxwell's equations, Oxford University Press, 2003.
[17] S. Adam, P. Arbenz, R. Geus, P. Arbenz, Eigenvalue solvers for electromagnetic fields in cavities, Technical Report 275, Institute of Scientific Computing, ETH *zü*rich, 1997.
[18] J. H. Lee, T. Xiao, and Q. H. Liu, A 3-D Spectral-Element Method Using Mixed-Order Curl Conforming Vector Basis Functions for Electromagnetic Fields, IEEE Trans. Microw. Theory Tech., 54 (2006), 437-444.
[19] M. Luo, Q. H. Liu, and Z. Li, Spectral element method for band structures of two-dimensional anisotropic photonic crystals, Phys. Rev. E 79, 026705 (2009), 1-8.
[20] N. Liu, Y. Tang, X. Zhu, L. Tobón and Q. H. Liu, Higher-order Mixed Spectral Element Method for Maxwell Eigenvalue Problem, IEEE International Symposium on Antennas and Propagation (APS 2013).
[21] P. Monk, on the p and hp extension of Nédélec's curl-conforming elements. J. Comp. Appl. Math., 53 (1994), 117-137.
[22] M. Suri, on the stability and convergence of higher-order mixed finite element methods for second-order elliptic problems, Math. Comp., 54 (1990), 1-19.
[23] R. Hiptmair, Finite elements in computational electromagnetism, Acta Numerica, 11 (2002), 237-339.
[24] A. N. Bespalov, Finite element method for the eigenmode problem of a RF cavity resonator, Sov. J. Numer. Anal. Appl. Math. Model., 3 (1988), 163-178.
[25] S. C. Brenner, F. Li and L. Sung, A Locally Divergence-free Interior Penalty Method for Two-dimensional Curl-curl Problems, SIAM J. Numer. Anal., 46 (2008), 1190-1211.
[26] http://perso. univ-rennes1. fr/monique. dauge/core/index. html.
[27] Z. P. Tanner, S. Savage, D. R. Tanner, and A. F. Peterson, Two-dimensional singular vector elements for finite-element analysis, IEEE Trans. Microw. Theory Tech., 46 (1998), 178-184.
[28] R. D. Graglia, and G. Lombardi, Singular higher order complete vector bases for finite methods, IEEE Trans. Antennas Propagat., 52 (2004), 1672-1685.
[29] O. A. Peverini, G. Addamo, G. Virone, R. Tascone, and R. Orta, A Spectral-Element Method for the Analysis of 2-D Waveguide Devices With Sharp Edges and Irregular Shapes, IEEE Trans. Microw. Theory Tech., 59 (2011), 1685-1695.

https://doi.org/10.4208/cicp.230113.140814a Published online by Cambridge University Press